Communication

FSS Sandwiched Dual-Frequency Reflectarray for Mobile Communication Applications

Jianfeng Li [1] , **Liangliang Mao** [1,*] **and Tianling Zhang** [2]

1   Department of Electronics, Lishui University, Lishui 323000, China
2   School of Electronic Engineering, Xidian University, Xi'an 710071, China
*   Correspondence: lsxymll@lsu.edu.cn

Abstract: Sandwiched frequency selective surface (FSS) is proposed as an additional reflection surface for a dual-frequency reflectarray system. The range of reflection phase for a reflectarray depends on the substrate thickness sensitively. Usually, a tradeoff between the smooth linear level and the wide reflection phase range is needed, especially for a dual-frequency system. By inserting an FSS between the ground plane and the reflecting element layer, a selective plane for the dual-frequency band is provided. For the higher frequency band, the FSS layer is a reflection plane. For the lower frequency band, it is transparent and the reflection plane is changed into the metal ground plane. A dual-band reflectarray with a scattering angle of 30 degrees is simulated and measured to validate this concept.

Keywords: reflectarray; frequency selective surface; dual-frequency

1. Introduction

A microstrip reflectarray antenna consists of a planar array of microstrip elements which are printed on a grounded substrate and illuminated by a primary feed source [1]. Comparing with the conventional parabolic reflector antenna, reflectarray combines the advantages of phased arrays and reflectors. Reflectarray rapidly becomes an attractive alternative. A number of reflectarray antennas have been developed since the 1980s. It has achieved wide applications and has many advantages, such as being of low profile and volume, surface-mountable and easy to deploy [1–20]. In modern wireless communication system such as in 5G/6G base stations or point-to-point communication systems, reflectarray antennas with plane structures can be installed conveniently on building walls or ceilings to reflect beams for covering different areas, especially for blind spots.

A typical reflectarray consists of a number of reflecting elements, as shown in Figure 1a. A progressive phase shift can be obtained using a certain tuning when illuminated by a primary source [1–6]. For a reflectarray, designing the reflection phase for the element is the key aspect during the design procedure. Many phase adjustment techniques have been reported in the literature: element rotation, using stubs lines, variable size and so on [1–9]. However, the phase range relies on the substrate thickness sensitively. For a traditional reflectarray with a single-layer substrate, the achievable reflection phase range is approximated:

$$360° \times (1.0 - kt/\pi) \tag{1}$$

where t is the thickness of the substrate and k is the wavenumber in the substrate [4]. It can be seen clearly from Formula (1) and Figure 1b that a thinner substrate offers a wider reflection phase range. Unfortunately, this is achieved at the cost of a high nonlinear relationship between the element size and reflection phases. A rapid phase change around the patch resonance makes the reflectarray design difficult for manufacturing errors. On the other hand, by increasing the thickness of the substrate, a much smoother variation of the reflection phase can be obtained. In the meantime, a narrower phase range arises. The insufficient reflection phase range makes practical designs unfeasible.
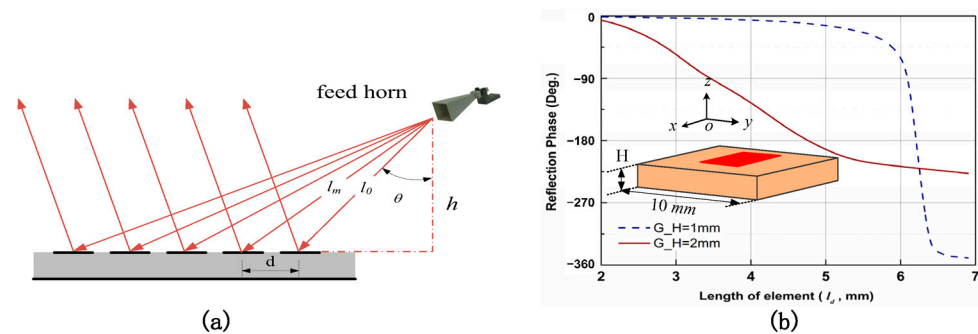
Figure 1. (**a**) Configuration of traditional reflectarray. (**b**) Reflection phase response for different substrates.

Usually, the reflectarray realized by using a single metal plane structure is suitable for a single frequency case or a limited frequency band. Furthermore, it is difficult to work in a wide scanning angle case, as a wide phase range would be needed [1–4]. In our current research, dual-frequency systems are required for modern multimedia communication applications. Additionally, the interval between the two operating frequencies is relatively large. Single substrate may be too thin to have a smooth phase range for a lower frequency resulting slope. In the meantime, it may be too thick for higher frequency to obtain enough phase range. Generally, a tradeoff between the smooth linear level and the wide phase range is needed.

The design of dual-band reflectarray antennas with high performance is one of the major considerations for multimode reflectarray design [5–10]. One of the most common approaches for dual-band application is to use a multi-layer reflectarray. However, the top layer blocks the signal form the other layer, and this technique has a probability that the materials will physically interfere with each other as their sizes are changed to obtain the required reflection phases. In [5], a dual-frequency reflectarray using a dual layer ring element working at 7.3 GHz and at 31.75 GHz was designed and reported by C. Han et al. The highest efficiencies measured were 46% at 7.3 GHz and 38% at 31.75 GHz, respectively. As described in the literature, the efficiency drop at the Ka band is caused by the interference of the C band layer. M.R Chaharmir et al. proposed another dual-frequency reflectarray working at 7.3 GHz and at 31.75 GHz [6]. Backed-FSS is utilized as the reflection plane at the Ka band. Two reflectarray layers were used, which also cause the problem of interference with each other. Another technique is using elements of two working frequency bands printed on the same layer. By using this technique, the blockage of the top layer in a multi-layer dual-band operation can be eliminated. However, the reflection phase of a reflectarray relies on the thickness of the substrate sensitively. That means wide and smooth phase range can be hardly obtained at both frequencies simultaneously.

In our research, a concept for a reflectarray design using a sandwiched FSS structure is proposed to solve the dual-band problem. To simultaneously obtain a larger reflection phase range, a smooth reflection phase curve and dual operating frequency bands, an additional FSS layer is sandwiched between the metal ground plane layer and the reflectarray element layer. For the incident wave, the FSS layer can play the role of the reflecting plane for a higher frequency band. Lastly, for the lower frequency band, this FSS layer is transparent and the reflection plane acts as the metal ground plane. A dual-band and dual-polarization reflectarray which comprises cross dipole elements and sandwiched FSS layer is designed and measured to validate this concept. Smooth and wide reflection phase ranges are achieved at both working frequency bands (12 GHz and 16 GHz). A 7 × 11 element reflectarray is fabricated to demonstrate the performance.

2. Reflectarray Design and Structure

To meet the requirements of dual-frequency and dual-polarization, cross-dipole elements were used for the present research. As shown in Figure 2a, for each cross-dipole

element, the horizontal dipole (*x*-direction) deals with the required reflection phase shift for the horizontally polarized incident wave at 12 GHz. The vertical dipole (*y*-direction) was designed for the vertical polarization at 16 GHz. The schematic diagram of the FSS sandwiched reflectarray is illustrated in Figure 2. Double substrates were used as shown in Figure 2b. The metal ground plane was the bottom of the first substrate (substrate 1, single metal). The top layer of the second substrate (substrate 2) was the reflectarray element layer. 7×11 elements with a size of 70×110 mm^2 were designed. The FSS layer was etched on the other side of substrate 2 with structure of loops linked by stripe lines. As shown in Figure 2b, the FSS layer was sandwiched between the reflectarray element layer and the metal layer. The thicknesses of two substrates were $h_1 = 0.8$ mm, $h_2 = 1.6$ mm, respectively. The permittivity was selected as 2.5 for both substrates.

(a)　Schematic diagram
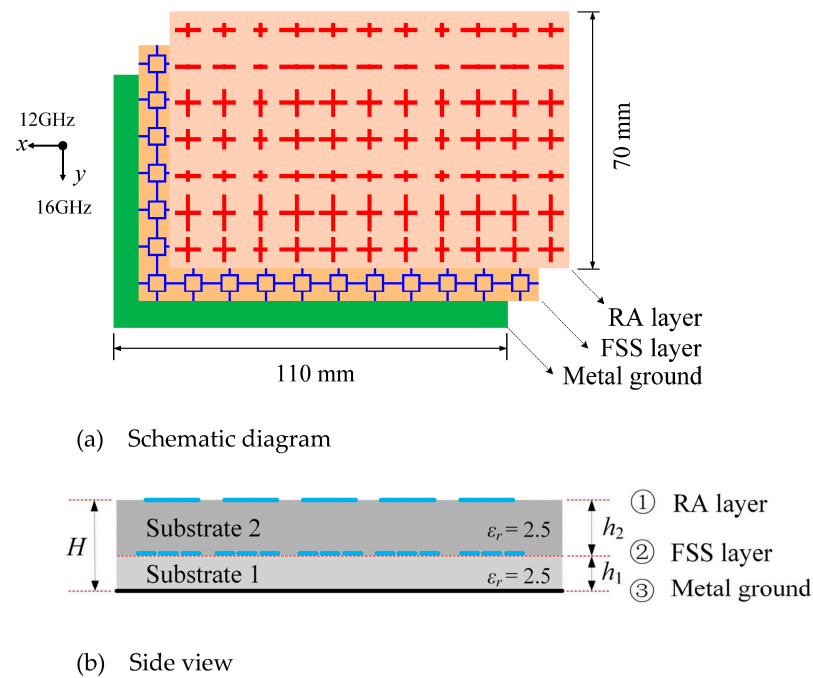
(b)　Side view

Figure 2. Schematic diagram and side view of the FSS sandwiched reflectarray.

To analyze the reflection phase characteristics of the unit cell, an infinite periodic model was performed using HFSS simulation with normal incidence. The periodic boundary condition (PBC) was set around the model and Floquet's ports were used, as shown in Figure 3a.
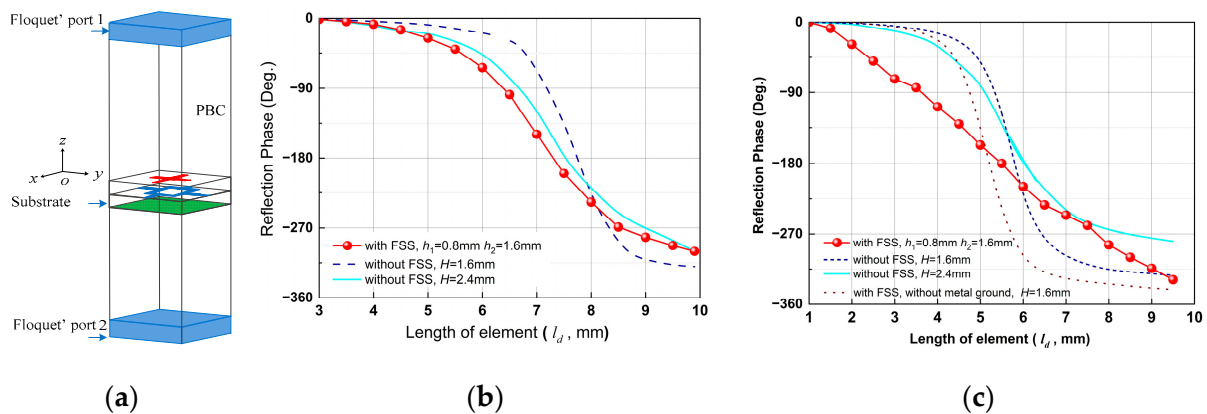
Figure 3. (**a**) Reflection phase methodology. (**b**) Relation between dipole length and reflection phase at 12 GHz. (**c**) Relation between dipole length and reflection phase at 16 GHz.

In a lower operating frequency (12 GHz), as can be seen in Figure 3b, if there is only a metal ground plane with a distance of 1.6 mm ($H = 1.6$ mm) from the reflectarray element layer (RA layer), the curve of the reflection phase shows a rapid variation around the resonance and a slow variation off resonance. When the metal ground is set to the distance of 2.4 mm ($H = 2.4$ mm), a smoother phase variation phase range can be obtained. However, the distance of 2.4 mm is too thick for 16 GHz, as depicted in Figure 3c. For the case of $H = 2.4$ mm without FSS, the phase variation is smooth but phase range is limited to less than 280°, which is not enough for the design.

When the FSS layer is inserted, the reflectarray has a frequency selected reflection ground. Thus, for the lower operating frequency (12 GHz), the FSS layer is invisible and the reflection plane acts as the metal ground of substrate 1. For the other working frequency (16 GHz), the inserted FSS is a PEC-like layer, from which the incidence field can be directly reflected.

From Figure 3c, it can be observed that smooth phase ranges (more than 300 degree) are obtained at both the lower and upper frequency by using the FSS sandwiched structure. At 16 GHz, a wider phase range can be obtained with inserted FSS. If the metal ground plane is replaced by FSS for $H = 1.6$ mm, a similar phase response can be obtained. For the case of $H = 2.4$ mm, FSS and the ground plane comprise a whole reflection structure. Due to the interaction between them, the FSS layer must be properly optimized. The final optimized FSS element has an inner loop length of 4.5 mm. As shown in Figure 3c, a more linear performance is obtained with the inserted FSS layer at the upper operating frequency.

The FSS element geometry is sketched in Figure 4; the adjacent loop elements are connected with a strip line. The size and shape of the FSS were optimized for a perfect transparent layer at the lower working frequency and a perfect reflection layer at the upper working frequency. As demonstrated in Figure 4b, the −5 dB S11 band is less than 1.8 GHz at 16 GHz and the reflecting amplitude is less than −20 dB at 12 GHz. Furthermore, the reflection amplitude is about 0 dB at 16 GHz. Excellent transparent and reflection performances are obtained at the lower and upper frequency bands, respectively.

(a)　　　　　　　　　　　　　　　　　　　　　　　(b)
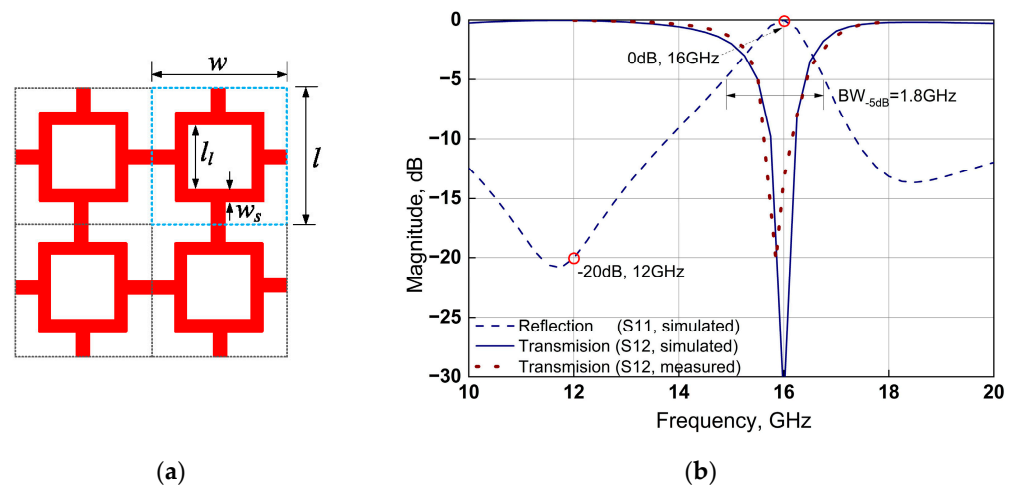
Figure 4. Modified square-loop element FSS (**a**) Geometry: Cell size: $l \times w = 10$ mm $\times$ 10 mm, length of loop: $l_l = 4.25$ mm, width of strip line: $w_s = 0.5$ mm. (**b**) S parameters V.S. frequencies for Modified FSS.

It is also noted that this concept is particularly suitable for a dual-frequency system with a large frequency interval, such as a 12 GHz and 24 GHz system, because the wavelengths at the two frequencies are very different.

According to the reflection phase response with the elements size depicted in Table 1, a 7 × 11 element reflectarray operating at 12 GHz (H-Polarization) and 16 GHz (V-Polarization) was fabricated to validate the concept (normal incidence and 30° desired scattering angle). The photographs of the reflectarray are shown in Figure 5. The top layer is a cross-dipole reflectarray element layer, as shown in Figure 5a. As the main beam

scans only in the xoz-plane (for 12 GHz)/yoz-plane (for 16 GHz), the dimensions of the cross-dipole length in x/y direction are the same within each column/row. The middle layer is the FSS layer, as shown in Figure 5b. Both of them were etched by using a milling and drilling LPKF prototype. The bottom layer is the metal ground of substrate 1 and not shown here, for clarity.

Table 1. Dipole length and compensation phase.

Column	Dipole Length (mm) x-Direction	Compensation Phase (Deg.) x-Direction	Dipole Length (mm) y-Direction	Compensation Phase (Deg.) y-Direction
1	7.00	0	6.77	−72
2	7.78	−72	9.82	−168
3	9.57	−144	3.00	96
4	3.80	144	5.45	0
5	6.23	72	7.62	−96
6	7.00	0	1.24	168
7	7.78	−72	3.78	72
8	9.57	−144	-	-
9	3.80	144	-	-
10	6.23	72	-	-
11	7.00	0	-	-
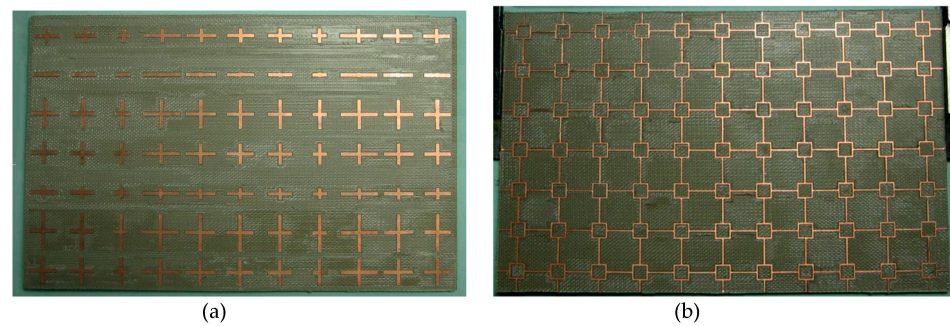
Figure 5. Photograph of a 7 × 11-element reflectarray using sandwiched FSS. (**a**) Top layer: cross-dipole elements layer. (**b**) Middle layer: Modified-loop FSS.

3. Fabrication of the Proposed Antenna and Measured Results

As shown in Figure 6, the measurement system was installed in an anechoic chamber. Around the measurement system, absorbing material was placed to reduce the edge effects and hide the horizontal supporting structure. As can be seen form Figure 6b, the vertical supporting arms for the DUT and the receiving antenna were made of a material with $\varepsilon_r \approx 1$.
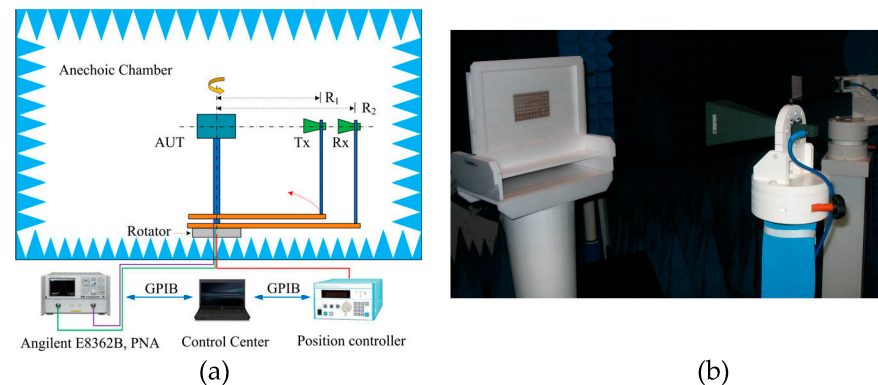
Figure 6. (**a**) Schematic of the reflectarray measurement system. (**b**) Photos of transmitting/receiving antennas and reflectarray under test.

Laser location devices were used to make sure the transmitting horn antenna, receiving antenna and the reflectarray under test were in the same horizon plane. The rotating position controller and Network analyzer (Agilent E8362B) were controlled by a computer program to change the AUT position and record the scattering pattern, respectively. Both of them were connected with a computer by GP-IP cables. The transmitting antenna (Tx) and receiving antenna (Rx) were a pair of horn antennas working at 12–18 GHz. The sizes of both horn antennas were the same. The aperture and the length of the horn antennas were 6.0×4.0 cm^2 and 15.0 cm, respectively. The distances from the reflectarray under test (RUT) to Rx and Tx were 1 m and 0.8 m, respectively. RUT and Tx/Rx had a distance of 1.2 m above the chamber ground. The transmitting horn rotated coherently with the reflective surface.

As depicted in Figure 7, the scattering patterns of the proposed reflectarray were measured in 1-degree increments in the azimuth plane. The main beam pointed at 29° at both operating frequencies. Considering the material losses and the effects introduced by the fabrication accuracy and the test rig in the actual test, there was a small shift from simulation. The maximum gains were 18.9 dBi and 21.2 dBi at 12 GHz(*xoz*-plane) and 16 GHz(*yoz*-plane), respectively. During the measurement, the transmitting and receiving horns overlapped at a range of $-15 \sim 15°$. Thus, the measured data in this range were not considered. All the above data demonstrate that the proposed antenna with optimal dimension performs excellently to meet the requirements of the desired application.

(**a**) 12 GHz　　　　　　　　　　　　　　　　　(**b**) 16 GHz

Figure 7. Scattering pattern of 11×7 element reflectarray. (**a**) 12 GHz. (**b**) 16 GHz.
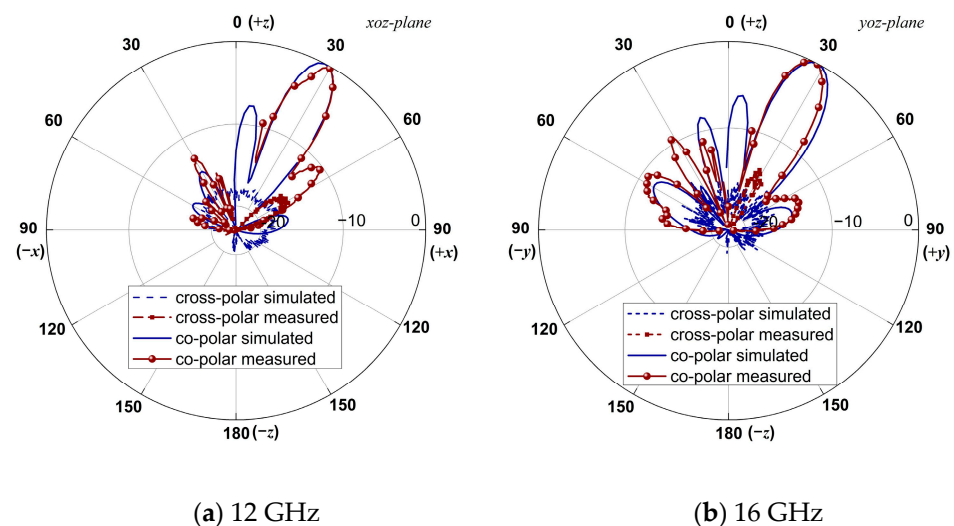
4. Conclusions

An FSS Sandwiched reflectarray was designed, fabricated and measured for dual-frequency and dual-polarization applications, which exhibits wide and smooth phase ranges at both lower and upper operating frequencies. A 11×7 element reflectarray using the sandwiched FSS was designed. Maximum gains of 18.9 dBi and 21.2 dBi at a 29° scattering angle were obtained at 12 GHz and 16 GHz, respectively. The proposed reflectarray can be used in the applications of 5G/6G base stations and point-to-point communication systems to provide fast data transfer. This concept can also be used for blind elimination in high-building downtown districts.

Institutional Review Board Statement: The study did not require ethical approval.

Informed Consent Statement: The study did not involve humans.

Data Availability Statement: The data presented in this study are available on request from the corresponding author.

Conflicts of Interest: The authors declare no conflict of interest.

References

1. Huang, J.; Encinar, J.A. *Reflectarray Antennas*; JohnWiley & Sons: Hoboken, NJ, USA, 2008.
2. M De Rioja, E.M.; de Rioja, D.M.; López-Sáez, R.; Linares, I.; Encinar, J.A. High-Efficiency Polarizer Reflectarray Antennas for Data Transmission Links from a CubeSat. *Electronics* **2021**, *10*, 1802. [CrossRef]
3. Zhou, M.; Sørensen, S.B.; Brand, Y.; Toso, G. Doubly Curved Reflectarray for Dual-Band Multiple Spot Beam Communication Satellites. *IEEE Trans. Antennas Propag.* **2020**, *68*, 2087–2096. [CrossRef]
4. Tsai, F.C.E.; Bialkowski, M.E. Designing a 161-element Ku-band microstrip reflectarray of variable size patches using an equivalent unit cell waveguide approach. *IEEE Trans. Antennas Propag.* **2003**, *51*, 2953–2962. [CrossRef]
5. Han, C.; Rodenbeck, C.; Huang, J.; Chang, K. A c/ka dual frequency dual layer circularly polarized reflectarray antenna with microstrip ring elements. *IEEE Trans. Antennas Propag.* **2004**, *52*, 2871–2876. [CrossRef]
6. Chaharmir, M.; Shaker, J.; Legay, H. Dual-band ka/x reflectarray with broadband loop elements. *Microw. Antennas Propag.* **2010**, *4*, 225–231. [CrossRef]
7. Encinar, J. Design of two-layer printed reflectarrays using patches of variable size. *IEEE Trans. Antennas Propag.* **2001**, *49*, 1403–1410. [CrossRef]
8. Smith, T.; Gothelf, U.V.; Kim, O.S.; Breinbjerg, O. An FSS-Backed 20/30 GHz circularly polarized reflectarray for a shared aperture L- and Ka-band satellite communication antenna. *IEEE Trans. Antennas Propagat.* **2014**, *62*, 661–668. [CrossRef]
9. Martinez-De-Rioja, E.; Encinar, J.; Barba, M.; Florencio, R.; Boix, R.R.; Losada-Torres, V. Dual Polarized Reflectarray Transmit Antenna for Operation in Ku- and Ka-Bands With Independent Feeds. *IEEE Trans. Antennas Propag.* **2017**, *65*, 3241–3246. [CrossRef]
10. Deng, R.; Xu, S.; Yang, F.; Li, M. An FSS-Backed Ku/Ka Quad-Band Reflectarray Antenna for Satellite Communications. *IEEE Trans. Antennas Propag.* **2018**, *66*, 4353–4358. [CrossRef]
11. De Rioja, D.M.; de Rioja, E.M.; Rodriguez-Vaqueiro, Y.; Encinar, J.A.; Pino, A.; Arias, M.; Toso, G. Transmit–Receive Parabolic Reflectarray to Generate Two Beams per Feed for Multispot Satellite Antennas in Ka-Band. *IEEE Trans. Antennas Propag.* **2021**, *69*, 2673–2685. [CrossRef]
12. Yu, Z.Y.; Zhang, Y.H.; He, S.Y.; Gao, H.T.; Chen, H.T.; Zhu, G.Q. A Wide-Angle Coverage and Low Scan Loss Beam Steering Circularly Polarized Folded Reflectarray Antenna for Millimeter-Wave Applications. *IEEE Trans. Antennas Propag.* **2022**, *70*, 2656–2667. [CrossRef]
13. Prado, D.R.; López-Fernández, J.A.; Barquero, G.; Arrebola, M.; Las-Heras, F. Fast and Accurate Modeling of Dual-Polarized Reflectarray Unit Cells Using Support Vector Machines. *IEEE Trans. Antennas Propag.* **2018**, *66*, 1258–1270. [CrossRef]
14. Zhou, M.; Sørensen, S.B.; Kim, O.S.; Jørgensen, E.; Meincke, P.; Breinbjerg, O. Direct Optimization of Printed Reflectarrays for Contoured Beam Satellite Antenna Applications. *IEEE Trans. Antennas Propag.* **2013**, *61*, 1995–2004. [CrossRef]
15. Niccolai, A.; Beccaria, M.; Zich, R.E.; Massaccesi, A.; Pirinoli, P. Social Network Optimization Based Procedure for Beam-Scanning Reflectarray Antenna Design. *IEEE Open J. Antennas Propag.* **2020**, *1*, 500–512. [CrossRef]
16. Ning, B.; Chen, Z.; Chen, W.; Du, Y.; Fang, J. Terahertz Multi-User Massive MIMO With Intelligent Reflecting Surface: Beam Training and Hybrid Beamforming. *IEEE Trans. Veh. Technol.* **2021**, *70*, 1376–1393. [CrossRef]
17. Capozzoli, A.; Curcio, C.; Liseno, A. CUDA-based particle swarm optimization in reflectarray antenna synthesis. *Adv. Electromagn.* **2020**, *9*, 66–74. [CrossRef]
18. Nayeri, P.; Yang, F.; Elsherbeni, A.Z. *Reflectarray Antennas: Theory, Designs and Applications*; Wiley Online Library: Hoboken, NJ, USA, 2018.
19. Nayeri, P.; Yang, F.; Elsherbeni, A.Z. Beam-Scanning Reflectarray Antennas: A technical overview and state of the art. *IEEE Antennas Propag. Mag.* **2015**, *57*, 32–47. [CrossRef]
20. Beccaria, M.; Niccolai, A.; Zich, R.E.; Pirinoli, P. Shaped-Beam Reflectarray Design by Means of Social Network Optimization (SNO). *Electronics* **2021**, *10*, 744. [CrossRef]